Lymph node cortical sinus organization and relationship to lymphocyte egress dynamics and antigen exposure

Irina L. Grigorova[a,1,2], Mikhail Panteleev[b,c], and Jason G. Cyster[a,2]

[a]The Howard Hughes Medical Institute and Department of Microbiology and Immunology, University of California, San Francisco, CA 94143; [b]Center for Theoretical Problems of Physico-Chemical Pharmacology, Russian Academy of Sciences, Moscow 125167, Russia; and [c]National Research Center for Hematology, Russian Academy of Medical Sciences, Moscow 125167, Russia

Edited by Max D. Cooper, Emory University, Atlanta, GA, and approved October 13, 2010 (received for review July 9, 2010)

Recent studies have identified cortical sinuses as sites of sphingosine-1-phosphate receptor-1 ($S1P_1$)-dependent T- and B-cell egress from the lymph node (LN) parenchyma. However, the distribution of cortical sinuses in the entire LN and the extent of lymph flow within them has been unclear. Using 3D reconstruction and intravital two-photon microscopy we describe the branched organization of the cortical sinus network within the inguinal LN and show that lymphocyte flow begins within blunt-ended sinuses. Many cortical sinuses are situated adjacent to high endothelial venules, and some lymphocytes access these sinuses within minutes of entering a LN. However, upon entry to inflamed LNs, lymphocytes rapidly up-regulate CD69 and are prevented from accessing cortical sinuses. Using the LN reconstruction data and knowledge of lymphocyte migration and cortical sinus entry dynamics, we developed a mathematical model of T-cell egress from LNs. The model suggests that random walk encounters with lymphatic sinuses are the major factor contributing to LN transit times. A slight discrepancy between predictions of the model and the measured transit times may be explained by lymphocytes undergoing a few rounds of migration between the parenchyma and sinuses before departing from the LN. Because large soluble antigens gain rapid access to cortical sinuses, such parenchyma–sinus shuttling may facilitate antibody responses.

antigen capture | inflammation | interstitial fluid | laminar flow

Lymphocyte recirculation between blood, lymphoid organs, and lymph is essential for immune surveillance. T and B lymphocytes get into LNs from the blood through high endothelial venules (HEVs); they then move into the T zone and B-cell follicles, respectively, and migrate there in a stromally guided random walk. If no antigenic stimuli have been encountered, lymphocytes leave into the efferent lymphatics after a characteristic residence time in murine lymph nodes (LNs) of 6–10 h for T cells and 12–24 h for B cells (1–3). During some immune responses, egress of naive lymphocytes from LNs is transiently blocked by IFNα/β. This egress "shutdown" has been modeled by systemic treatment with double-stranded mRNA mimetic polyinosine-polycytidylic acid [poly(I:C)] that induces secretion of IFNα/β, as well as with lymphocytic choriomeningitis virus (LCMV) infection (4). The induced block in egress partially depends on lymphocyte-intrinsic up-regulation of CD69. CD69 is a transmembrane protein that negatively regulates sphingosine-1-phosphate receptor-1 ($S1P_1$), a receptor for sphingosine-1-phosphate (S1P) that is required for lymphocyte egress (4, 5). However, the stage at which CD69 inhibits cell departure from the LNs has not been fully defined.

Recent studies of murine LNs identified lymphatic vascular endothelial gene-1 (LYVE-1)$^+$ cortical sinuses as sites of T- and B-cell exit from the LN parenchyma (6–8). Using intravital two-photon laser scanning microscopy (TPLSM), it was shown that intrinsic expression of $S1P_1$ on T lymphocytes regulates their access into the cortical sinuses, whereas fluid flow within these sinuses mediates their retention and passive transport toward the medulla and efferent lymphatic (7). However, cortical sinuses often appear packed with cells (6, 9–12) and it has been unclear whether all of these structures exhibit fluid flow.

A systematic view of lymphocyte recirculation through LNs under normal and inflamed conditions requires better understanding of (*i*) the distribution of the lymphocyte exit sites in the LNs (LYVE-1$^+$ sinuses with flow in them) relative to entry sites (HEVs), (*ii*) the time within which lymphocytes could access and transmigrate into the exit sites after arrival into the LNs, (*iii*) the fraction of cells that return back into LN parenchyma from LYVE-1$^+$ sinuses, and (*iv*) the regulation of these processes by local inflammation. In this work we have undertaken studies to address these questions. By confocal microscopy we obtained a 3D reconstruction of HEV and LYVE-1$^+$ sinus distribution in an entire inguinal lymph node (ILN). By TPLSM we find that multiple blunt-ended cortical sinuses show evidence of cell flow. Large soluble antigen gains efficient access into cortical sinuses, providing further evidence for fluid flow in these structures while also suggesting that they may function as sites of antigen acquisition by B cells. Many cortical sinuses are proximal to HEVs, and newly entered lymphocytes have rapid access into these exit sites. In a model of local inflammation induced by poly(I:C), naive lymphocytes coming into an inflamed LN rapidly up-regulate CD69 and are blocked from accessing cortical sinuses. We developed a quantitative model of T-cell egress from ILNs that incorporates the experimentally measured distribution of the cortical sinuses, known T-cell motility parameters, and sinus entry efficiency. We find that for this model to accurately predict lymphocyte residence time in the LN, it is necessary to propose that lymphocytes shuttle between the parenchyma and sinuses a few times before reaching the efferent lymphatics.

Results

Blunt-Ended Cortical Sinuses Exhibit Flow. To gain quantitative information about the positioning and morphology of cortical sinuses in murine LNs, we performed a 3D reconstruction of LYVE-1$^+$ sinuses and HEVs in an entire ILN by serial sectioning; staining for LYVE-1, CD31 (PECAM1), and CD4; and analyzing by confocal microscopy. Image stacks were collected from adjacent

Author contributions: I.L.G. and J.G.C. designed research; I.L.G. performed research and modeling analysis of LN egress; I.L.G. and J.G.C. analyzed data; M.P. designed the model of antigen diffusion against liquid flow and performed dynamic simulations; and I.L.G., M.P., and J.G.C. wrote the paper.

The authors declare no conflict of interest.

This article is a PNAS Direct Submission.

Freely available online through the PNAS open access option.

[1]Present address: Department of Microbiology and Immunology, University of Michigan Medical School, Ann Arbor, MI 48109.

[2]To whom correspondence may be addressed. E-mail: igrigor@umich.edu or jason.cyster@ucsf.edu.

This article contains supporting information online at www.pnas.org/lookup/suppl/doi:10.1073/pnas.1009968107/-/DCSupplemental.

20- to 30-μm sections and then compiled into a single file. This reconstruction demonstrated the presence of multiple blunt-ended sinuses that started near HEVs in interfollicular regions or at the follicle/T-zone boundary (Fig. 1), in agreement with previous studies (12, 13). Several connecting sinuses that extended from the subcapsular sinus (SCS) to medullary sinuses were also identified and usually were located adjacent to a B-cell follicle as well as passing near HEVs (Fig. 1 and Movies S1 and S2). The 3D map obtained of the LYVE-1$^+$ structures allowed sinus distribution with respect to HEVs and the total sinus surface area to be measured, providing necessary parameters for egress modeling, as described further below. As an approach to examine whether the blunt-ended cortical sinuses showed evidence of cell flow, we determined the axis ratio of CD4 T cells that were within the lumen of the sinus and not touching the wall, within the lumen and touching the wall, or within the parenchyma near the sinus (Fig. 2 *A* and *B*). This analysis showed that most of the cells within the lumen and free from the sinus wall had a smaller axis ratio than the other cells, indicating they were more rounded and thus likely caught and retained in fluid flow (Fig. 2 *A* and *B*) (7). We then asked whether we could detect cells flowing within blunt-ended structures using intravital TPLSM. In a series of experiments we observed a steady lymph flow in the SCS (detected by faint autofluorescence of the lymph and by the large diameter of the SCS) for the first 2–3 h after the surgery, but after this time the flow became more variable. Studies in animal models and in humans have shown that prolonged anesthesia is associated with a reduction in lymph flow (14, 15). When the TPLSM analysis was performed within the first 2–3 h after surgery, many blunt-ended sinuses had cells flowing in them in the direction of the medulla (Movies S3 and S4). We therefore suggest that blunt-ended sinuses act as lymphocyte-retaining exit sites.

High Molecular Weight Antigen Gains Rapid Access to Cortical Sinuses. Because we detected slowly flowing cells in many cortical sinuses, we speculated that lymph-borne antigens accessing medullary sinuses may diffuse via the lymph to cortical sinuses. To test this possibility, we injected mice with phycoerythrin-coupled hen egg lysozyme (HEL-PE) (~300 kDa), an antigen complex that is too large to access the LN parenchyma via conduits (16). To facilitate visualization of the antigen without the complication of loss during tissue preparation, we first transferred two populations of reporter B cells that are able to bind HEL with high affinity: wild-type MD4 Ig-transgenic B cells that localize in follicles and CXCR5-deficient MD4 Ig-transgenic B cells that localize to interfollicular and follicle-proximal T-zone regions. These are the sites where most of the cortical sinuses are situated. Three minutes after injection of HEL-PE into the footpad, many MD4 B cells in the cortical sinuses, medulla, and SCS had bound the antigen, whereas the majority of MD4 B cells in the parenchyma were unstained (Fig. 3*A*). Similar labeling was observed in ILNs 20–30 min after s.c. injection of HEL-PE in the flank and the base of the tail (Fig. 3*B*). The more rapid labeling after footpad compared with flank injection may reflect greater hydrostatic pressure in the former injection site, leading to more rapid movement of antigen through the afferent lymph. At 40–60 min after s.c. injection of HEL-PE, MD4 B cells in proximity to the cortical, medullary, and SC sinuses of the draining ILN had bound the antigen (Fig. 3*C*). The rate of HEL-PE appearance in LN sinuses and capture by MD4 B cells varied between animals, likely reflecting variations in drainage from the injection site. However, a similar sequence of labeling in sinuses and surrounding parenchyma was seen in multiple experiments (Fig. S1). HEL-PE gave brighter staining in the medulla than in cortical sinus regions after both s.c. and footpad injections (Fig. 3 and Fig. S1). This result is consistent with access of HEL-PE to cortical sinuses by diffusion from the medullary sinuses against the direction of the slowly flowing

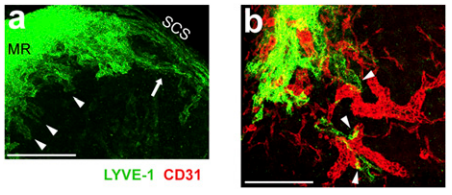

Fig. 1. Projection view of LYVE-1$^+$ sinuses and HEVs in ILN. (*A*) 3D view through an ILN from its cortical side, obtained by reconstruction of serial sections stained with anti-LYVE-1 (green) and imaged by confocal microscopy. LYVE-1 antibody stained cortical, medullary, and subcapsular sinuses (SCS), as well as macrophages in the medullary region. MR, medullary region between the two lobes of ILN. (Scale bar, 300 μm.) Data are representative of ILN serial section analysis from three mice (Movie S1). (*B*) Projection view of a 46-μm-thick section of ILN 70 μm underneath the capsule from the cortical side, stained to detect LYVE-1 (green) and CD31 (red) and imaged by confocal microscopy. (Scale bar, 300 μm.) Data are representative of ILN serial section analysis from two mice (Movie S2). Arrowheads in *A* and *B* indicate blunt-ended sinuses. Arrow in *A* indicates a sinus connected to the SCS at both ends.

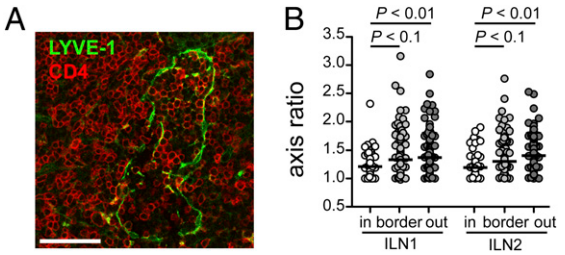

Fig. 2. Lymphocytes within blunt-ended cortical sinuses are rounded. (*A*) Confocal microscopy image showing a section from a blunt-ended LYVE-1$^+$ sinus, stained for LYVE-1 (green) and CD4 (red). (Scale bar, 50 μm.) (*B*) Axis ratio of CD4 T cells inside blunt-ended LYVE-1$^+$ cortical sinuses. Data are shown for T cells inside and not touching the sinus wall (white circle), touching the sinus wall (light gray circle), and outside of the sinuses (dark gray circle). Data are combined from two serial reconstructions of ILNs (two mice), and in each, four different blunt-ended structures were analyzed. Medians are shown by horizontal lines.

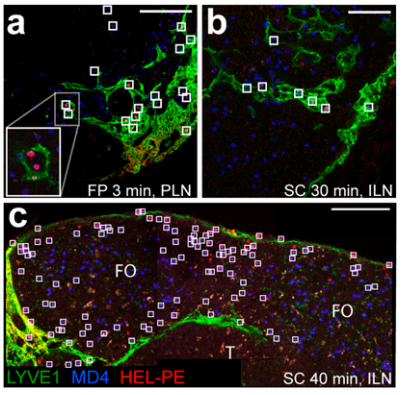

Fig. 3. Emergence of s.c. injected HEL-PE in cortical sinuses. (*A*–*C*) Confocal images of peripheral LN sections, stained to detect LYVE-1 (green) and the transferred MD4 or MD4 CXCR5$^{-/-}$ B cells (by HEL-A647, blue). (*A*) Projection view of 6.4-μm-thick section of a popliteal LN with MD4 CXCR5$^{-/-}$ B cells 3 min after injection of HEL-PE into the footpad. (Scale bar, 100 μm.) (*B*) Projection view of 6.4-μm-thick section of ILN with MD4 and MD4 CXCR5$^{-/-}$ B cells 30 min after s.c. injection of HEL-PE into the flanks and the base of the tail. (Scale bar, 50 μm.) (*C*) Combined view of three adjacent sections of ILN (19- to 26-μm-thick projection views) with MD4 B cells, 40 min after s.c. injection of HEL-PE into the flanks and base of the tail. (Scale bar, 100 μm.) Squares indicate MD4 and MD4 CXCR5$^{-/-}$ B cells stained with HEL-PE. FO, follicle; T, T zone.

cortical sinus lymph. In support of this hypothesis, dynamic calculations of diffusion against laminar liquid flow (*SI Materials and Methods*) suggest that protein antigens with molecular mass ~300 kDa should rapidly spread into the sinuses if the liquid flow rate is comparable to or even a few fold faster than the experimentally measured flow rate of cells in the sinuses (7) (Fig. S2).

Previous studies have shown that the small molecular weight antigen HEL-A647 gains rapid access to LN follicles either directly from the SCS or via conduits (17, 18), although how this antigen distributes with respect to cortical sinuses was not determined. Two to 5 min after footpad injection of HEL-A647, popliteal LNs showed a wave front-like labeling pattern of the MD4 B cells that propagated through the follicles away from the capsule and the brightly stained medulla (Fig. S3). Although the extent of MD4 B-cell staining in the cortical sinuses was variable within this time period, they always appeared stained where the HEL-A647 wave front from the follicles or from the medulla reached the sinuses. Overall, the similar kinetics of HEL-A647 localization into the follicles and cortical sinuses suggest that the cortical sinuses themselves are not a preferential path for LN access by small antigens. These data also suggest that HEL-A647 diffusion through the follicles or spreading through sparse follicular conduits (17, 18) occurs before spread through the T-zone conduit network (16, 19). By 5–10 min after HEL-A647 footpad injection, most MD4 B cells proximal to or within the T zone were also stained.

In our previous analysis of T-cell behavior in cortical sinuses, we noted that some cells moved from the sinus back into the parenchyma, although this behavior was less profound in regions with flow (7). Here we observed examples of B cells migrating from cortical sinus regions with flow back into the parenchyma (Movies S4 and S5). These observations suggest some amount of lymphocyte "shuttling" between sinuses and parenchyma, as also suggested by the quantitative analysis below, and might provide a mechanism for B-cell return into the parenchyma after an encounter with large soluble antigens in the sinuses.

Rapid Access of Lymphocytes into Cortical Sinuses. The close proximity of cortical sinuses to HEVs (Fig. 1) led us to ask how quickly cells entering LNs through HEVs can gain access to the sinuses. To address this question mice were injected with lymphocytes i.v. followed by LN section analysis to determine positioning of the transferred cells. No examples of direct transmigration from HEVs into sinuses were observed. The cells arriving in the LN at the junction of HEVs with lymphatic sinuses appeared aligned along the wall of the sinus (Fig. 4*A*). However, at 20 and 30 min after injection, many transferred lymphocytes were detected within the sinuses (Fig. 4*B*, Movie S6). These observations suggest that $S1P_1$, which is down-regulated on lymphocytes in the blood (20), resensitizes sufficiently within 20 min of lymphocyte entry to the LN parenchyma for their productive transmigration into cortical sinuses.

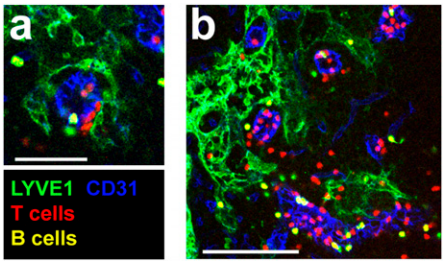

Fig. 4. Rapid access of lymphocytes into cortical sinuses. (*A* and *B*) Confocal images of peripheral LN sections from mice, i.v. injected 30 min earlier with T cells, labeled with CMTMR (red), and B cells, colabeled with CMTMR and CFSE (yellow), and stained to detect LYVE-1 (green) and CD31 (blue). (*A*) Projection view of 1.9-μm-thick section. (Scale bar, 50 μm.) (*B*) Projection view of 10-μm-thick section (Movie S6). (Scale bar, 100 μm.) Data are representative of two experiments.

Lymphocyte Exclusion from Cortical Sinuses During Inflammation. The observed ability of lymphocytes to get into the exit sites shortly after their entry into the LN implies that a fraction of lymphocytes may go into the efferent lymphatics before surveying for antigen in the parenchyma. However, antigen presentation in lymphoid organs is often accompanied by inflammation. We therefore attempted to assess what happens to the newly arriving cells in locally inflamed LNs. IFNα/β induced in response to poly(I:C) injection causes up-regulation of lymphocyte CD69 and inhibition of the egress-promoting function of $S1P_1$ (4). Six hours after systemic treatment with poly(I:C), many cortical sinuses in peripheral LNs were partially or fully collapsed (Fig. S4*A*). To test whether sinus collapse occurs because of the displacement of CD69 up-regulated lymphocytes from the exit structures, we asked whether lymphocyte-intrinsic deficiency in CD69 would reverse the phenotype. Indeed, analysis of [$CD69^{-/-} \mapsto$ WT] and [$CD69^{+/+} \mapsto$ WT] bone marrow (BM) chimeras showed that at 6 h after poly(I:C) treatment, cortical sinuses in [$CD69^{-/-} \mapsto$ WT] BM chimeras were less collapsed than in [$CD69^{+/+} \mapsto$ WT] BM chimeras (Fig. S4*B*). Moreover, quantitative analysis of $CD69^{-/-}$ and $CD69^{+/+}$ T and B cells cotransferred into wild-type recipient mice showed that $CD69^{-/-}$ cells were enriched in the cortical sinuses relative to the $CD69^{+/+}$ cells at 6 h after poly(I:C) treatment (Fig. 5*A–D*). On the basis of these data, we infer that CD69 up-regulation reduces lymphocyte entry into cortical sinuses. This reduction results in a partial collapse of the cortical sinuses, similar to what was reported in mice treated with FTY720 or in lymphatic sphingosine kinase-deficient mice (8, 21).

To address how quickly CD69 is up-regulated on lymphocytes arriving into an inflamed LN, we induced localized LN inflammation by footpad injection of poly(I:C) with simultaneous control injection of PBS into the contralateral footpad (Fig. 5*E*). By 6 h after injection, cells in poly(I:C) draining popliteal LNs started up-regulating CD69 whereas in the contralateral LN (and the other peripheral LNs) CD69 up-regulaton did not occur. Analysis of CD69 up-regulation by lymphocytes arriving into the inflamed popliteal LN showed that B cells and CD8 T cells started up-regulation of CD69 by 30–60 min after their arrival (Fig. 5*F*). The onset of CD69 up-regulation was a little delayed in CD4 T cells, taking place between 60 and 90 min after their entry (Fig. 5*E*). These data show that CD69 up-regulation by lymphocytes in the inflamed LN is rapid compared with the median LN residence time and thus could significantly reduce the chance of potentially antigen-reactive lymphocytes undergoing premature exit from an inflamed LN.

Quantitative Model of T-Cell Egress from ILN. In a currently envisioned model of lymphocyte egress from LNs, naive lymphocytes can encounter $LYVE\text{-}1^+$ sinuses while moving in the LN by a stromally guided random walk. Upon the encounter they either turn back in the parenchyma or transmigrate into the exit structure, where they can become captured by flow and carried into the efferent lymphatics (6, 7). However, whether (*i*) distribution of the entry and exit sites, (*ii*) frequency of transmigration into the exit site upon contact, and (*iii*) lymphocyte motility within the T zone are sufficient to explain the experimentally measured kinetics of lymphocyte egress from the LN is unclear. To test this, we developed two quantitative models of T-cell egress from the ILN, using two different approaches to model T-cell motility within the lymph node: the simple model (SM) (22) and the conditional probability model (CPM) (*SI Materials and Methods*). On the basis of these quantitative models and the experimentally measured parameters (*i–iii*), we calculated the rate of lymphocyte entry into the sinuses

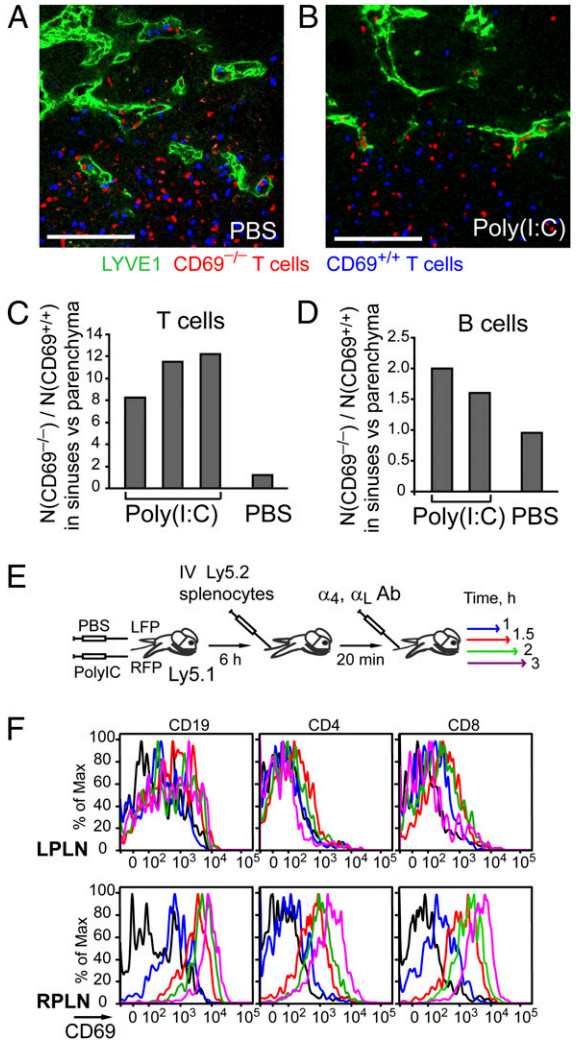

Fig. 5. Exclusion of CD69^{hi} lymphocytes from cortical sinuses during inflammation. (*A*–*D*) Analysis of confocal images of peripheral LN sections from mice that had received cotransferred CD69$^{+/+}$ (labeled with CFSE, blue) and CD69$^{-/-}$ (labeled with CMTMR, red) T or B lymphocytes and were treated for the last 6 h with PBS or poly(I:C). (*A* and *B*) Representative sections, stained to detect LYVE-1 (green). (Scale bars, 100 μm.) (*C* and *D*) Quantitative analysis showing relative changes in the ratio of the CD69$^{-/-}$ to CD69$^{+/+}$ (*C*) T-cell or (*D*) B-cell numbers in the LYVE-1^{+} cortical sinuses compared with the (*C*) T zone and (*D*) follicles. In each mouse at least ten 10- to 30-μm-thick (375 × 375 μm) sections containing cortical sinuses were analyzed. (*E* and *F*) Kinetics of CD69 up-regulation by T and B lymphocytes after their entry into locally inflamed popliteal LNs. (*E*) Schematic of the experiment. Six hours after poly(I:C) injection into the right footpad (RFP) and PBS into the left footpad (LFP), Ly5.1 recipient mice were i.v. injected with Ly5.2 lymphocytes. After 20 min, further entry of lymphocyte into the LNs was blocked by i.v. injection of α_4- and α_L-specific antibodies. (*F*) Flow cytometric analysis of CD69 up-regulation by the transferred cells in inflamed right popliteal LN (RPLN, *Lower*) or control LNs (LPLN, *Upper*) at 1 h (blue), 1.5 h (red), 2 h (green), and 3 h (violet) after transfer. Data shown are representative of three experiments performed at 6 h and one experiment at 18 h.

(Fig. 6 and Fig. S7) and compared it with an experimentally measured residence time of T cells in ILNs.

Both the SM and the CPM models of lymphocyte egress predict that ~30% of T cells arriving in the ILN through HEVs encounter the exit structures within the first 30 min, and by 2 h half of them encounter the sinuses at least once (Fig. 6 *A* and *B*). The newly arriving lymphocytes have a higher probability of encountering the sinuses compared with the cells residing in the ILN for >2 h (Fig. 6 *A* and *B*, note the slope of the curve), due to the proximity of the cortical sinuses to HEVs. Overall, the CPM predicts an ~20–25% faster rate of T-cell encounter with the sinuses and egress compared with the SM (Fig. 6). Under an assumption that the efficiency of lymphocyte transmigration into the sinuses does not change with time following their arrival in the ILN, the expected half-life of T cells in the ILN (before they transmigrate into LYVE-1^{+} sinuses) is predicted to be ~4–5 h (Fig. 6 *C* and *D*). This value would be only slightly delayed if the cells were unable to transmigrate into the sinuses (for example, due to S1P$_1$ resensitization requirements) within the first 15 or 30 min after their entry (Fig. 6 *C* and *D*).

In addition to the quantitative modeling, we performed a volumetric analysis of T-cell access to LYVE-1^{+} sinuses (*SI Materials and Methods*). This analysis is based on the ratio of the cumulative surface area of the sinuses facing the T zone to the entire volume of the T zone (extracted from the representative ILN) and on the experimentally measured T-cell transmigration frequency and the time T cells spent in contact with the sinuses. In contrast to the quantitative modeling, volumetric analysis does not depend on the distribution of the entry sites and T-cell motility. The range of half-lives for T-cell transmigration into LYVE-1^{+} sinuses estimated by volumetric analysis is either faster than or comparable to the predictions of the quantitative model (*SI Materials and Methods* and Fig. S8), with both of them suggesting a slightly faster rate of T-cell access into the sinuses from the T zone than the reported

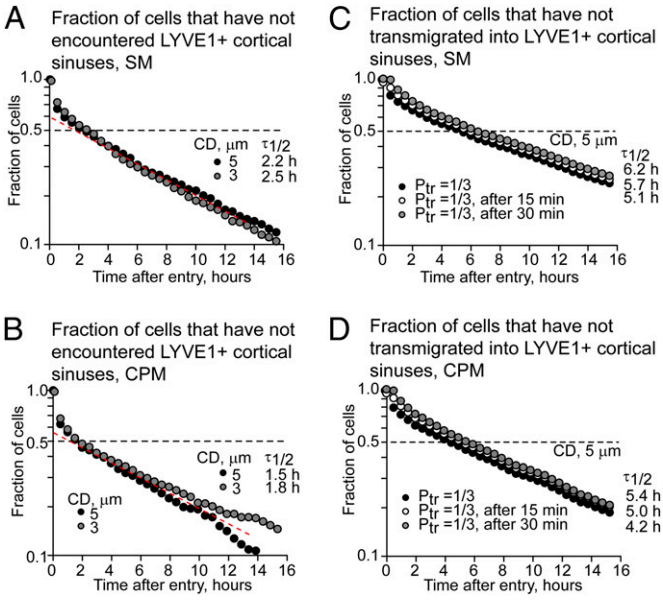

Fig. 6. Predictions of the quantitative models of lymphocyte entry into cortical sinuses in the ILN. Calculations were performed using T lymphocyte motility modeled as a simple random walk (SM) (*A* and *C*) or a conditional probability random walk (CPM) (*B* and *D*) and 3D reconstruction of HEVs and LYVE-1^{+} sinuses of a representative ILN. For description see *SI Materials and Methods*. (*A* and *B*) Fraction of T cells that have not encountered cortical LYVE-1^{+} sinuses at various times after cell arrival into the ILN through HEVs. Simulations were performed with minimal distance set to 2 μm and contact distance of 5 μm (black circles) and 3 μm (gray circles). The dashed red line indicates the region of constant probability of encountering LYVE-1^{+} sinuses between ~2 and 10 h after cell entry and higher probability of sinus contact before 2 h after entry. $\tau_{1/2}$, calculated half-life for the first encounters of cells with sinuses. (*C* and *D*) The fraction of cells that have not transmigrated into LYVE-1^{+} sinuses from the parenchyma if the probability of transmigration upon contact is 0.3. The probability of transmigration is constant (black circles), zero in the first 15 min after entry (white circles), or zero in the first 30 min after entry (gray circles). Simulations were performed with minimal distance set to 2 μm and contact distance of 5 μm. $\tau_{1/2}$, calculated half-life for cell transmigration into sinuses (Fig. S6).

rate of CD4 and CD8 T-cell exit from LNs (3). If the kinetics of lymphocyte exit from ILNs is tightly regulated (as would be expected on the basis of the previous report) (3), then the discrepancy between cell entry into the sinuses and egress from the ILN may be caused by overestimation of cell entry into some cortical sinuses. The frequency of T-cell transmigration into the sinuses was similar in various regions of ILNs imaged by TPLSM in four separate experiments (Fig. S5*A*) (7, 8). Therefore, we speculate that T-cell transmigration frequency does not vary a lot between various regions of the exit sites, although we cannot exclude its gradual variation over time (timer mechanism). For a timer mechanism to be relevant, it would have to operate over a long timescale, because we found little effect of reducing sinus entry efficiency for the 15–30 min after entry. However, multiple examples of lymphocyte return into parenchyma from the sinuses led us to propose an alternative mechanism that might contribute to lymphocyte transit time within LNs. Lymphocyte recirculation between the sinuses and parenchyma was experimentally observed before and in this work (Movies S4 and S5) (7, 8), especially in regions of the sinuses without flow or where the flow of the cells was restrained by macrophages close to the capsule. The experimental assessment of the physiological extent of lymphocyte return from the cortical sinuses back into the parenchyma may be somewhat ambiguous due to reduction in the fluid flow occurring during the intravital imaging. Estimations made with the quantitative model of T-cell egress suggest that to achieve an agreement between the calculated rate of cell entry into the sinuses and the experimentally measured half-life of T cells in the ILNs (8–9 h) (3), about half of the T cells that transmigrate into the sinuses should return back into the T zone.

Discussion

In this study we demonstrate that blunt-ended cortical sinuses in LNs contain many rounded lymphocytes that are moving toward medullary sinuses. We suggest that the presence of lymph flow in cortical sinuses promotes the rounding up and capture of cells that have entered in an $S1P_1$-dependent manner, reducing their propensity to migrate back into the parenchyma and helping ensure they reach medullary sinuses and exit the LN. Using quantitative information about major LN exit sites, the volume of the T zone, and the established migration parameters of LN T cells, we estimate LN transit times that are quite close to the measured values, suggesting that these are the major parameters determining naive lymphocyte transit time. Although the model predicts egress times slightly faster than those that have been measured, our dynamic analysis shows that some cells do return to the parenchyma from sinuses, providing a likely explanation for the discrepancy.

The pathways of fluid flow into cortical sinuses have not been well defined. Conduits have been suggested to channel lymph arriving in the SCS to HEVs for return to blood circulation (12, 19). Because many blunt-ended cortical sinuses initiate near HEVs, it seems likely that such channeling also delivers lymph to cortical sinuses, and some tracer studies are consistent with this interpretation (23–25). In TPLSM experiments we observed simultaneous decreases in the amount of afferent lymph in the SCS (suggested by collapse of the ILN capsule after a few hours of intravital imaging) and in the cell flow rate in cortical sinuses, consistent with the possibility of fluid delivery from the SCS via the parenchyma and/or conduits. Due to the detection of higher protein concentrations in efferent compared with afferent lymph, the close proximity between HEVs and lymphatics, and their positive staining for aquaporin, it was previously suggested that lymph may flow from the blunt-ended cortical sinuses into the blood (12). However, we believe the more parsimonious explanation of the available data are that there is fluid accumulation by both HEVs and cortical sinuses. Moreover, LN capillaries may contribute to the formation of interstitial fluid in the LN such that there is some local passage of fluid from the blood into the cortical sinuses (26).

A typical view of the LN immune surveillance function is that lymphocytes enter the LN and then survey for antigen or antigenic peptides on dendritic cells (DCs), a process that may require hours. However, the immune surveillance function of LNs might be better considered in a hierarchical way, where the primary level of surveillance is for LN inflammation and the secondary level is for antigen or peptides displayed by DCs. With this view, a key requirement for successful immune surveillance is that the inflamed state of the LN is detected rapidly by entering lymphocytes. We show that when T and B cells enter an inflamed LN, CD69 is induced within an hour and access to cortical sinuses is strongly blocked. The collapse of many cortical sinuses in LNs responding to poly(I:C) that occurred as a result of CD69 induction in the lymphocyte is similar to the emptying of sinuses that is seen within hours of treatment with the $S1P_1$-modulating drug, FTY720 (8, 21), and suggests that the presence of lymphocytes within the sinuses is important for holding them open. This result also suggests that there is a lack of structural components, such as extracellular matrix tethers, to hold them open and implies that the amount of fluid flow within the structures is influenced by their cellular content.

Recent studies identified a number of paths by which antigens arriving in LNs can reach B cells. Whereas small antigens (<70 kDa) can gain direct access to follicles via the SCS floor or through conduits, particulate and opsonized antigens can be captured and displayed to B cells by SCS macrophages or transported to areas near follicles by DCs (18, 27, 28). The ability of large protein antigens to gain rapid access to cortical sinuses, most likely by diffusion in the lymph, suggests a unique mode of B cell encounter with antigen. Interestingly, although the pathway is predicted to be accessible for big proteins/protein complexes, for viral particles this access should be orders of magnitude less efficient (Fig. S2). We demonstrate that cognate B cells within or adjacent to cortical sinuses rapidly acquire the large HEL-PE antigen complex. The visualization of some B cells moving from cortical sinuses back into the parenchyma, and the suggestion from the modeling analysis that many of the T cells that enter sinuses return to the parenchyma at least once, supports the possibility that this is a relevant pathway of local B-cell antigen encounter. Under inflammatory conditions, antigen exposure by entry into lymphatic sinuses will be antagonized by CD69, but B cells may continue to probe sinuses in an $S1P_1$-indpendent manner (7), allowing for continued exposure to sinusoidal antigen. DCs might also acquire large soluble antigens, perhaps including viral antigens (29), by sampling cortical sinus fluids. B cells are occasionally observed migrating on the luminal side of the SCS (8, 30), and consistent with direct exposure of such cells to SCS lymph, some antigen-labeled cognate B cells were detected in the SCS within minutes of HEL-PE injection. Thus, all of the sinuses in the LN may serve as sites for B-cell encounter with large soluble antigens during their period of drainage into the LN.

Materials and Methods

Mice. Six- to 12-wk-old Ly5.1 (CD45.2) and Ly5.2 (CD45.1) C57BL/6 mice were from either the National Cancer Institute or Jackson Laboratories. C57BL/6 Tg(UBC-GFP)30Scha/J (004353) were from Jackson Laboratories. MD4 (31), $CXCR5^{-/-}$ (32), and $CD69^{-/-}$ (33) mice were from internal colonies. [$CD69^{+/+}$ ↦ WT] and [$CD69^{-/-}$ ↦ WT] BM chimeras were generated by reconstitution of irradiated Ly5.2 mice with bone marrow from $CD69^{+/+}$ and $CD69^{-/-}$ mice, as described (6). Immunizations and treatments with poly(I:C) were performed as described in *SI Materials and Methods*. Animals were housed in a specific pathogen-free environment in the Laboratory Animal Research Center at University of California (San Francisco), and all experiments conformed to ethical principles and guidelines approved by the Institutional Animal Care and Use Committee.

Cell Isolation and Flow Cytometry. T and B cells were isolated from spleen, peripheral and mesenteric LNs, and purified as described (7). Purities were typically >95%. Lymphocyte preparations before adoptive transfer and lymph node cells postimaging were stained with various fluorochrome-conjugated

antibodies from BD Pharmingen as described (7), and data were acquired on a FACS Calibur (BD) and analyzed with FlowJo software (Treestar).

Reagents. HEL was conjugated to Alexa-Fluor 647 (Molecular Probes labeling kit) and purified using BioSpin 6 columns (Bio-Rad Laboratories) or to phycoerythrin and purified as described (34).

Cell Labeling and Adoptive Transfers. Donor cells were labeled, where indicated, with 10 μM of 5-(and-6)-(((4-chloromethyl)benzoyl)amino) tetramethylrhodamine (CMTMR) (Invitrogen/ Molecular Probes) or 5 μM of carboxyfluorescein diacetate succinimidyl ester (CFSE) (Invitrogen/Molecular Probes), in DMEM containing 1% FBS for 25 min at 37 °C, and then washed by spinning through a layer of FBS. Labeled or unlabeled cells were adoptively transferred into the tail vein of recipient mice.

Confocal Microscopy and Intravital Two-Photon Microscopy. Techniques used were similar to those previously described (7, 30). See *SI Materials and Methods* for details.

Development of the quantitative model of T-cell exit from ILNs and volumetric analysis were performed as described in *SI Materials and Methods*.

Statistical Analysis. All statistical analysis was performed in GraphPad Prism (GraphPad Software). For comparison of multiple nonparametric datasets we used the Kruskal–Wallis test followed by Dunn's posttest comparison between multiple groups.

ACKNOWLEDGMENTS. We thank T. Nakayama (Chiba University, Japan) for CD69$^{-/-}$ mice; M. Lipp (The Max-Delbrück Center for Molecular Medicine, Berlin) for CXCR5$^{-/-}$ mice; P. Beemiller, K. Suzuki, and X. Wang for technical help; Fred Schaufele for help with confocal microscopy; H. Li for critical feedback on the mathematical model; and T. Arnon and K. Suzuki for comments on the manuscript. I.L.G. was supported by an Irvington Institute Fellowship of the Cancer Research Institute and an Immunology program National Institutes of Health training grant. J.G.C. is an Investigator of the Howard Hughes Medical Institute. This work was supported in part by National Institutes of Health Grants AI45073 and AI74847.

1. Ford WL, Simmonds SJ (1972) The tempo of lymphocyte recirculation from blood to lymph in the rat. *Cell Tissue Kinet* 5:175–189.
2. Westermann J, Puskas Z, Pabst R (1988) Blood transit and recirculation kinetics of lymphocyte subsets in normal rats. *Scand J Immunol* 28:203–210.
3. Tomura M, et al. (2008) Monitoring cellular movement in vivo with photoconvertible fluorescence protein "Kaede" transgenic mice. *Proc Natl Acad Sci USA* 105:10871–10876.
4. Shiow LR, et al. (2006) CD69 acts downstream of interferon-alpha/beta to inhibit S1P1 and lymphocyte egress from lymphoid organs. *Nature* 440:540–544.
5. Bankovich AJ, Shiow LR, Cyster JG (2010) CD69 suppresses sphingosine-1-phosophate receptor-1 function through interaction with membrane helix 4. *J Biol Chem* 285: 22328–22337.
6. Pham TH, Okada T, Matloubian M, Lo CG, Cyster JG (2008) S1P1 receptor signaling overrides retention mediated by G alpha i-coupled receptors to promote T cell egress. *Immunity* 28:122–133.
7. Grigorova IL, et al. (2009) Cortical sinus probing, S1P1-dependent entry and flow-based capture of egressing T cells. *Nat Immunol* 10:58–65.
8. Sinha RK, Park C, Hwang IY, Davis MD, Kehrl JH (2009) B lymphocytes exit lymph nodes through cortical lymphatic sinusoids by a mechanism independent of sphingosine-1-phosphate-mediated chemotaxis. *Immunity* 30:434–446.
9. Söderström N, Stenström A (1969) Outflow paths of cells from the lymph node parenchyma to the efferent lymphatics—observations in thin section histology. *Scand J Haematol* 6:186–196.
10. Kelly RH (1975) Functional anatomy of lymph nodes. I. The paracortical cords. *Int Arch Allergy Appl Immunol* 48:836–849.
11. Bélisle C, Sainte-Marie G (1981) Tridimensional study of the deep cortex of the rat lymph node. III. Morphology of the deep cortex units. *Anat Rec* 199:213–226.
12. Ohtani O, Ohtani Y (2008) Structure and function of rat lymph nodes. *Arch Histol Cytol* 71:69–76.
13. He Y (1985) Scanning electron microscope studies of the rat mesenteric lymph node with special reference to high-endothelial venules and hitherto unknown lymphatic labyrinth. *Arch Histol Jpn* 48:1–15.
14. Dahan A, Mendelman A, Amsili S, Ezov N, Hoffman A (2007) The effect of general anesthesia on the intestinal lymphatic transport of lipophilic drugs: Comparison between anesthetized and freely moving conscious rat models. *Eur J Pharm Sci* 32: 367–374.
15. Yamada S, Kubo M, Hayashida Y (1988) Lymph flow dynamics into the thoracic duct of the rat. *Jpn J Physiol* 38:729–733.
16. Gretz JE, Norbury CC, Anderson AO, Proudfoot AE, Shaw S (2000) Lymph-borne chemokines and other low molecular weight molecules reach high endothelial venules via specialized conduits while a functional barrier limits access to the lymphocyte microenvironments in lymph node cortex. *J Exp Med* 192:1425–1440.
17. Pape KA, Catron DM, Itano AA, Jenkins MK (2007) The humoral immune response is initiated in lymph nodes by B cells that acquire soluble antigen directly in the follicles. *Immunity* 26:491–502.
18. Roozendaal R, et al. (2009) Conduits mediate transport of low-molecular-weight antigen to lymph node follicles. *Immunity* 30:264–276.
19. Lämmermann T, Sixt M (2008) The microanatomy of T-cell responses. *Immunol Rev* 221:26–43.
20. Lo CG, Xu Y, Proia RL, Cyster JG (2005) Cyclical modulation of sphingosine-1-phosphate receptor 1 surface expression during lymphocyte recirculation and relationship to lymphoid organ transit. *J Exp Med* 201:291–301.
21. Pham TH, et al. (2010) Lymphatic endothelial cell sphingosine kinase activity is required for lymphocyte egress and lymphatic patterning. *J Exp Med* 207:17–27.
22. Beauchemin C, Dixit NM, Perelson AS (2007) Characterizing T cell movement within lymph nodes in the absence of antigen. *J Immunol* 178:5505–5512.
23. Anderson AO, Shaw S (1993) T cell adhesion to endothelium: The FRC conduit system and other anatomic and molecular features which facilitate the adhesion cascade in lymph node. *Semin Immunol* 5:271–282.
24. Gretz JE, Anderson AO, Shaw S (1997) Cords, channels, corridors and conduits: Critical architectural elements facilitating cell interactions in the lymph node cortex. *Immunol Rev* 156:11–24.
25. Sixt M, et al. (2005) The conduit system transports soluble antigens from the afferent lymph to resident dendritic cells in the T cell area of the lymph node. *Immunity* 22: 19–29.
26. Bélisle C, Sainte-Marie G (1990) Blood vascular network of the rat lymph node: Tridimensional studies by light and scanning electron microscopy. *Am J Anat* 189: 111–126.
27. Gonzalez SF, Pitcher LA, Mempel T, Schuerpf F, Carroll MC (2009) B cell acquisition of antigen in vivo. *Curr Opin Immunol* 21:251–257.
28. Phan TG, Gray EE, Cyster JG (2009) The microanatomy of B cell activation. *Curr Opin Immunol* 21:258–265.
29. Gonzalez SF, et al. (2010) Capture of influenza by medullary dendritic cells via SIGN-R1 is essential for humoral immunity in draining lymph nodes. *Nat Immunol* 11: 427–434.
30. Phan TG, Green JA, Gray EE, Xu Y, Cyster JG (2009) Immune complex relay by subcapsular sinus macrophages and noncognate B cells drives antibody affinity maturation. *Nat Immunol* 10:786–793.
31. Goodnow CC, et al. (1988) Altered immunoglobulin expression and functional silencing of self-reactive B lymphocytes in transgenic mice. *Nature* 334:676–682.
32. Förster R, et al. (1996) A putative chemokine receptor, BLR1, directs B cell migration to defined lymphoid organs and specific anatomic compartments of the spleen. *Cell* 87:1037–1047.
33. Murata K, et al. (2003) CD69-null mice protected from arthritis induced with anti-type II collagen antibodies. *Int Immunol* 15:987–992.
34. Suzuki K, Grigorova I, Phan TG, Kelly LM, Cyster JG (2009) Visualizing B cell capture of cognate antigen from follicular dendritic cells. *J Exp Med* 206:1485–1493.